The Astronomical Journal, 164:168 (15pp), 2022 October https://doi.org/10.3847/1538-3881/ac8cff

A Deep and Wide Twilight Survey for Asteroids Interior to Earth and Venus

Scott S. Sheppard[1], David J. Tholen[2], Petr Pokorný[3,4,5], Marco Micheli[6], Ian Dell'Antonio[7], Shenming Fu[7,8], Chadwick A. Trujillo[9], Rachael Beaton[10,11], Scott Carlsten[10], Alex Drlica-Wagner[12,13], Clara Martínez-Vázquez[14,15], Sidney Mau[16], Toni Santana-Ros[17,18], Luidhy Santana-Silva[19], Cristóbal Sifón[20], Sunil Simha[21], Audrey Thirouin[22], David Trilling[9], A. Katherina Vivas[15], and Alfredo Zenteno[15]

[1] Earth and Planets Laboratory, Carnegie Institution for Science, 5241 Broad Branch Road NW, Washington, DC, 20015, USA; ssheppard@carnegiescience.edu
[2] Institute for Astronomy, University of Hawai'i, Honolulu, HI, 96822, USA
[3] Department of Physics, The Catholic University of America, Washington, DC, 20064, USA
[4] Astrophysics Science Division, NASA Goddard Space Flight Center, Greenbelt, MD, 20771, USA
[5] Center for Research and Exploration in Space Science and Technology, NASA/GSFC, Greenbelt, MD, 20771, USA
[6] ESA NEO Coordination Centre, Largo Galileo Galilei, 1, I-00044 Frascati (RM), Italy
[7] Physics Department, Brown University, Box 1843, Providence, RI, 02912, USA
[8] NSF's National Optical-Infrared Astronomy Research Laboratory, 950 North Cherry Avenue, Tucson, AZ, 85719, USA
[9] Department of Astronomy and Planetary Science, Northern Arizona University, Flagstaff, AZ, 86011, USA
[10] Department of Astrophysical Sciences, Princeton University, 4 Ivy Lane, Princeton, NJ, 08544, USA
[11] The Observatories of the Carnegie Institution for Science, 813 Santa Barbara Street, Pasadena, CA, 91101
[12] Fermi National Accelerator Laboratory, P.O. Box 500, Batavia, IL, 60510, USA
[13] Department of Astronomy and Astrophysics, University of Chicago, Chicago, IL, 60637, USA
[14] Gemini Observatory, NSF's NOIRLab, 670 N. A'ohoku Place, Hilo, HI, 96720, USA
[15] Cerro Tololo Inter-American Observatory/NSF's NOIRLab, Casilla 603, La Serena, Chile
[16] Department of Physics, Stanford University, 382 Via Pueblo Mall, Stanford, CA, 94305, USA
[17] Departamento de Física, Ingeniería de Sistemas y Teoría de la Señal, Universidad de Alicante, Carr. de San Vicente del Raspeig, s/n, SE-03690 San Vicente del Raspeig, Alicante, Spain
[18] Institut de Ciéncies del Cosmos (ICCUB), Universitat de Barcelona (IEEC-UB), Carrer de Martí i Franqués, 1, SE-08028, Barcelona, Spain
[19] NAT-Universidade Cruzeiro do Sul/Universidade Cidade de São Paulo, Rua Galvão Bueno, 868, 01506-000, São Paulo, SP, Brazil
[20] Instituto de Física, Pontificia Universidad Católica de Valparaíso, Casilla 4059, Valparaíso, Chile
[21] University of California at Santa Cruz, 1156 High Street, Santa Cruz, CA, 95064 USA
[22] Lowell Observatory, 1400 W Mars Hill Road, Flagstaff, AZ, 86001, USA
Received 2022 June 8; revised 2022 August 15; accepted 2022 August 24; published 2022 September 29

Abstract

We are conducting a survey using twilight time on the Dark Energy Camera with the Blanco 4 m telescope in Chile to look for objects interior to Earth's and Venus' orbits. To date we have discovered two rare Atira/Apohele asteroids, 2021 LJ4 and 2021 PH27, which have orbits completely interior to Earth's orbit. We also discovered one new Apollo-type Near Earth Object (NEO) that crosses Earth's orbit, 2022 AP7. Two of the discoveries have diameters $\gtrsim$1 km. 2022 AP7 is likely the largest Potentially Hazardous Asteroid (PHA) discovered in about eight years. To date we have covered 624 square degrees of sky near to and interior to the orbit of Venus. The average images go to 21.3 mag in the *r* band, with the best images near 22nd mag. Our new discovery 2021 PH27 has the smallest semimajor axis known for an asteroid, 0.4617 au, and the largest general relativistic effects (53 arcsec/century) known for any body in the solar system. The survey has detected ~15% of all known Atira NEOs. We put strong constraints on any stable population of Venus co-orbital resonance objects existing, as well as the Atira and Vatira asteroid classes. These interior asteroid populations are important to complete the census of asteroids near Earth, including some of the most likely Earth impactors that cannot easily be discovered in other surveys. Comparing the actual population of asteroids found interior to Earth and Venus with those predicted to exist by extrapolating from the known population exterior to Earth is important to better understand the origin, composition, and structure of the NEO population.

Unified Astronomy Thesaurus concepts: Near-Earth objects (1092); Small Solar System bodies (1469); Atira group (111); Apollo group (58); Aten group (110); Earth trojans (438); Asteroids (72)

1. Introduction

The small body population in our solar system interior to Earth's and Venus' orbits has not been extensively explored to date because of the difficulty in observing near the glare of the Sun. Twilight observations near Venus' orbit from ground-based Earth telescopes occur at a very high airmass, with a bright sky background, poorer than average seeing, and with the objects of interest being at high phase angles during a short observational window. These factors create well over a magnitude of signal-to-noise loss when compared to observations overhead at night. This region of space is important for understanding the distribution of Near Earth Objects (NEOs) and objects that may have stable orbits in resonance with Venus.

One way to estimate the true number of small NEOs better is to include more objects found interior to Earth's orbit in population calculations, increasing the completion of orbital NEO types (Granvik et al. 2018; Harris & Chodas 2021). Currently the population models are biased toward NEOs found exterior to Earth's orbit as they are the easiest to find observationally. Only about 25 asteroids are known that have orbits completely interior to Earth's orbit and have well-determined orbits (called Atira or Apohele asteroids). This is compared to the thousands of known NEOs with orbits that

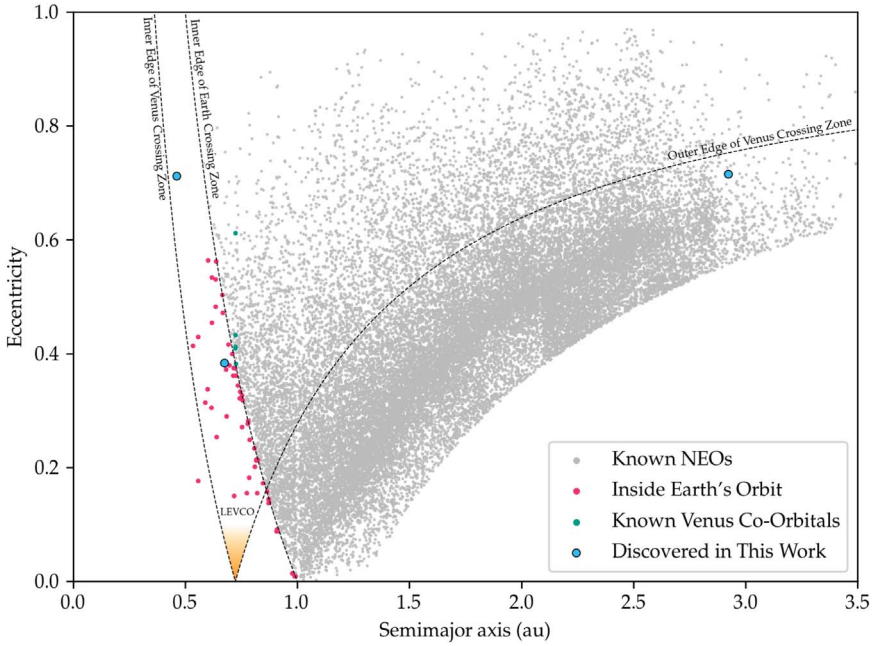

Figure 1. Known NEOs plotted with semimajor axis vs. eccentricity. The new discoveries from this survey are shown by big blue circles. The yellow area shows the region near Venus' orbit that dynamcially stable low-eccentricity Venus co-orbitals would be expected to be found, where no asteroid is known. All known asteroids with semimajor axes similar to Venus are on dynamically unstable, highly eccentric orbits that cross Earth's orbit (small green circles). Atira-type object orbits remain interior to Earth's orbit, shown as red circles to the left of the vertical dashed line starting at 1 au, which is the inner edge of the Earth crossing zone.

cross Earth's orbit such as Aten and Apollo NEOs with semimajor axes interior and exterior to Earth, respectively (Mainzer et al. 2014; Schunova-Lilly et al. 2017; Morbidelli et al. 2020).

Understanding the relative populations of objects with orbits interior to Earth versus exterior to Earth will help us understand how objects are transported throughout the inner solar system (Strom et al. 2015). In addition, disruption processes of NEOs, such as fragmenting from thermal stresses, breaking up from rotational excitation, or tidal disruption from passing near the Sun or planets can be analyzed by comparing the predicted number of NEOs found interior to Earth versus exterior to Earth and correlating this with the composition or type of objects found (Granvik et al. 2016). Such correlations and analysis will further yield insights into the structure and strength of the different types of NEO classes. Various internal stresses on NEOs such as tidal deformation and solar heating will cause more fragile asteroid compositions and structures to erode or break-up as they approach the planets and Sun (Li & Jewitt 2013; Ye & Granvik 2019).

In addition to NEOs, which are strongly influenced by the Earth, some objects found interior to Earth's orbit may exhibit strong influences from Venus. There are a few known well observed asteroids that have orbital periods similar to Venus': (322756) 2001 CK32, (524522) 2002 VE68, 2012 XE133, 2013 ND15, and 2015 WZ12 as well as some more recently discovered NEOs with semimajor axes near Venus' between 0.722 and 0.725 au: 2020 BT2, 2020 CL1, 2020 QU5, 2021 XA1, 2021 XO3, 2022 BL5, and 2022 CD (see Figures 1 and 2). All of these near-Venus co-orbital asteroids are dynamically unstable on million year timescales since they have high-eccentricity orbits that cross the orbit of the Earth (Mikkola et al. 2004; de la Fuente Marcos & de la Fuente Marcos 2012, 2013, 2014, 2017). The same situation has been found for the known co-orbitals of Earth (Brasser et al. 2004; Connors et al. 2011; Hui et al. 2021; Santana-Ros et al. 2022). The population of low-eccentricity Venus and Earth co-orbitals that are stable resonant objects may be small due to perturbations from terrestrial planets or nongravitational effects (Morais & Morbidelli 2006; Malhotra 2019; Pokorny & Kuchner 2021). There are no known satellites of Venus, likely because the Hill sphere of Venus is mostly dynamically unstable to long term satellites (Sheppard & Trujillo 2009). To date, the population of 1 km and smaller objects near Venus' orbit is relatively unconstrained observationally as most surveys in this region are only sensitive to larger objects.

Data from the two space missions HELIOS and STEREO indicate the presence of a narrow ring of dust in Venus' orbit (Leinert & Moster 2007; Jones et al. 2013). This Venus co-orbital dust ring could come from a population of low-eccentricity ($e < 0.3$) stable Venus resonant co-orbital objects (Pokorny & Kuchner 2019). These authors also found that about 8% of an initial population of Venus resonant objects remain stable for the age of the solar system. Thus, these putative low-eccentricity Venus resonant co-orbitals could be the leftover remnants of the planetesimals that formed near Venus, unlike most NEOs and high-eccentricity Venus co-orbitals that are believed to have recently escaped from the much further out main asteroid belt (Granvik et al. 2017). This theorized population of low-eccentricity Venus resonant objects has yet to be observationally ruled out since most surveys to date have not covered the large areas of sky to the faint depths needed to find such a population of low-eccentricity objects interior to Earth. This population could be too faint for small class telescopes to detect efficiently in the glare of the Sun as objects less than about 1 km in size would mostly be fainter than about 20th magnitude (Morbidelli et al. 2020; Masiero et al. 2020).

Surveys that have covered a significant portion of the sky looking for asteroids near Venus have used small class

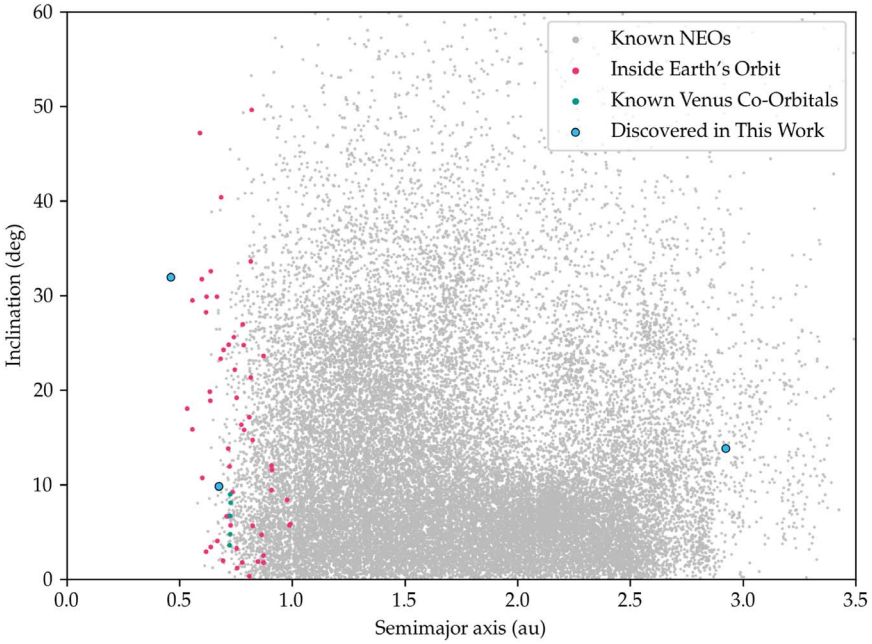

Figure 2. Same as Figure 1 but using inclination.

telescopes (Myhrvold 2016). Recently the 48 inch telescope Zwicky Transient Facility (ZTF; Ye et al. 2020) survey has done the most extensive search for asteroids near Venus. ZTF found the first ever asteroid that has an orbit entirely interior to Venus, (594913) 'Ayló'chaxnim (2020 AV2; Bolin et al. 2020), though the orbit is only stable for a few million years (Greenstreet 2020; de la Fuente Marcos & de la Fuente Marcos 2020; Bolin et al. 2022). This survey has covered several thousand square degrees of sky interior to Earth's orbit, but is limited in its discovery ability of smaller objects as it uses a 1.2 m telescope (Ye et al. 2020). Based on 'Ayló'chaxnim's absolute magnitude, it is likely a relatively large asteroid of ~1.5 km in size.

We performed a pilot survey in 2019 September to determine if a search for objects near Venus' orbit is feasible with the medium class Blanco 4 m telescope using the large field-of-view Dark Energy Camera (DECam), which is the largest sky area camera on a 4 m or larger telescope. We searched about 35 square degrees of sky some 40°–50° in elongation away from the Sun near the end of nautical and start of astronomical twilight time in the evening. The images went to over 21st mag in the *r* band and we were able to put some moderate limits on the size of any stable Venus resonant co-orbital population (Pokorny et al. 2020). Here we discuss an additional 589 square degrees of twilight sky near to and interior to Venus' orbit, yielding a total of 624 square degrees searched in the survey to date.

2. Observations

The twilight survey for objects near to and interior to Venus' orbit uses the DECam on the Cerro-Tololo Inter-American Observatory (CTIO) 4 meter Blanco telescope in Chile. DECam has 61 working science CCDs arranged in a circular type pattern at the prime focus of the telescope. Each CCD has 2048×4096 pixels with a pixel scale of about 0.264 arcseconds, yielding a field of view of about 2.7 square degrees per image (Flaugher et al. 2015). Images were calibrated by subtracting a median bias image and divided by a median dome flat.

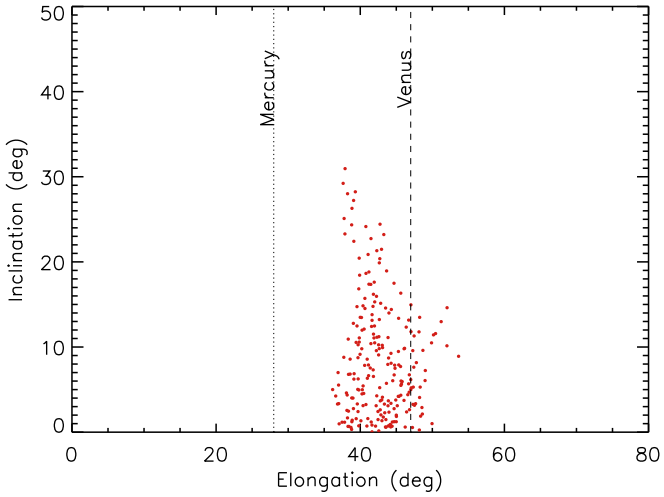

Figure 3. The twilight survey fields taken with DECam showing their elongation position from the Sun and inclination from the ecliptic. The maximum elongation from the Sun to Mercury and Venus are shown by vertical dotted and dashed lines, respectively.

Observations were obtained just after nautical twilight ends in the evening and just before nautical twilight begins in the morning. The Sun is usually between about −15 and −12 degrees below the horizon when the images are taken, giving about 10 minutes of observation time each twilight. Images were generally taken at airmasses between about 2.3 and 2.5, near the 23° elevation limit of the telescope. Most fields were observed near to or interior to Venus' orbit when projected onto the sky (Figure 3). The *r*-band filter with an exposure time of 28 s was used. With simultaneous readout and offsetting the telescope to the next position a few degrees away, it takes just under 1 minute between the start of two successive images. Two images of each field are taken separated by about 2–4 minutes. The images usually only had a background of a few

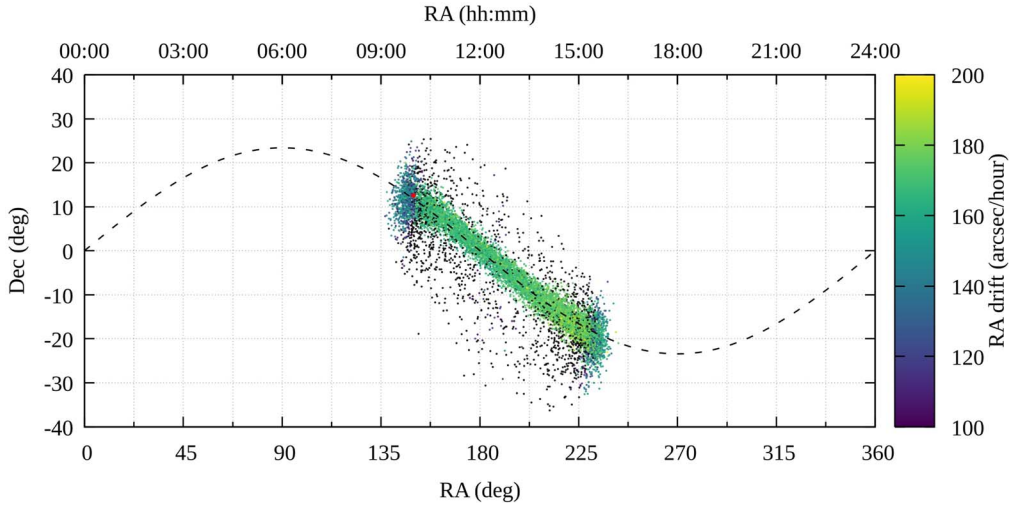

Figure 4. The R.A. and decl. of a hypothetical population of low-eccentricity, low-inclination, stable Venus co-orbital asteroids (Pokorny & Kuchner 2019) as they would appear on 2020 September 30 at 23:30 UT. Objects near Venus' orbit well interior to Earth's orbit would appear to move faster than about 100 arcseconds per hour, distinguishing them from more distant main belt asteroids that tend to move slower than 80 arcseconds per hour. The red dot shows Venus' location.

thousand counts, while the detector does not saturate until several tens of thousands of counts.

The depth of each image mostly depends on the seeing and the sky brightness. The signal-to-noise ratio of asteroids in the twilight images is generally worse than when observed exterior to Earth's orbit because of the high phase angles of the asteroids, bright background sky, and high airmass. In the twilight images taken near the Sun, the main belt asteriods are much farther away in our fields than when imaged in darker skies exterior to Earth's orbit. Thus, because of the relatively large distances of the main belt asteroids, our survey will not usually find unknown main belt asteroids.

An object that is interior to Earth's orbit will generally have an apparent motion of over 100 arcseconds per hour, with objects near Venus' orbit expected to show motions near 150 arcseconds per hour (Figure 4). The exposure time is limited by the fast motion of the objects, as an object with an apparent motion of 150 arcseconds per hour will start to show significant trailing after about 30 s. The survey used 28 s for the exposure time to limit any signal-to-noise trailing losses of the asteroids. The moving object search algorithm was the same as that used to find outer solar system objects (Trujillo et al. 2001; Sheppard et al. 2019) and it was set to flag any objects that were found to have an apparent motion faster than 75 arcseconds per hour. This allows us to identify easily the objects of interest that could be NEOs or Venus resonant co-orbitals while rejecting the many objects within the main asteroid belt and beyond, as their apparent motion is less than about 80 arcseconds per hour. Since some main belt asteroids have apparent motions faster than our 75 arcsecond per hour lower limit, we used the known main belt asteroids that we detected moving faster than 75 arcseconds per hour to help characterize our survey's detection efficiency.

We determined the limiting magnitude or depth to find moving objects in our survey fields based on two techniques. First, we determined to what magnitude we detected known main belt asteroids as well as known NEOs. Second, we implanted artificial moving objects into some fields to determine our moving object detection efficiency. The techniques are complementary and agreed to within a tenth of a magnitude of each other. The known main belt asteroids had their V-band Minor Planet Center magnitudes converted to r-band magnitudes using the simple conversion $V-r=0.2$ mag (Smith et al. 2002; Sheppard 2012; Sergeyev & Carry 2021). Artificial objects were placed in some of the fields ranging from 19th to 23rd mag in the r band with apparent motions as expected for NEOs between 80 and 170 arcseconds per hour. Because of the short time-base of only ~4 minutes between images and the short integration time of 28 s, we found no significant differences in our detection of objects with the fastest or slowest apparent motions.

We find that for the average field with a seeing of about 1.″4, we detected about 50% of artificially implanted objects for $m_r \sim 21.3$ mag, which is what we take as the overall limiting magnitude of the survey, though different nights had different limiting magnitudes as shown in Table 1 and Figure 5, with some of the best seeing fields reaching nearly 22nd mag in depth. The detection efficiency curve has a similar shape each night as shown in Figure 6, just shifted in m_r to the value as shown in Table 1, which mostly depended on the seeing. Figure 5 shows the limiting magnitude of each field versus the elongation of the field from the Sun. The survey was able to detect asteroids near Venus' orbit of only a few hundred meters in size assuming moderate albedos like S-type asteroids (Pokorny et al. 2020).

From Jedicke et al. (2016) we use Equation (15) to fit the detection efficiency curve shown in Figure 6: $\epsilon(m_r) = \epsilon_o[1 + \exp(m_r - r_{50\%}/r_{\rm width})]^{-1}$, where $r_{50\%}$ is the magnitude in the r band where the efficiency is 50%, ϵ_o is the maximum survey efficiency (i.e., the brightest object efficiency), and $r_{\rm width}$ is the magnitude range in m_r that the efficiency decreases from near 75% to 25%. We find $\epsilon_o = 0.95 \pm 0.01$, $r_{50\%} = 21.3$, and $r_{\rm width} = 0.19$.

As the survey was active every few nights, most of the asteroid recovery of new discoveries was done using DECam. D. Tholen also recovered new discoveries with the University of Hawaii 88 inch telescope and the Canada-France-Hawaii 3.6 m telescope (CFHT). The 6.5 m Baade–Magellan telescope at Las Campanas in Chile was also used in recovery observations as was the 1 meter global network of telescopes operated by Las Cumbres Observatory, mainly through the European Space Agency's (ESA) Planetary Defense Office (PDO).

Table 1
Observed Twilight DECam Fields

R.A.(J2000) hh:mm:ss	Decl.(J2000) dd:mm:ss	UT Date YYYY/MM/DD/hh:mm	Limiting (mag)	Seeing (arcseconds)
14:45:00	−17:30:00	2019/09/23/23:30	21.0	1.3
14:45:00	−19:30:00	2019/09/23/23:31	21.0	1.3
14:49:00	−17:30:00	2019/09/23/23:32	21.0	1.3
14:49:00	−19:30:00	2019/09/23/23:33	21.0	1.3
14:49:00	−15:30:00	2019/09/23/23:34	21.0	1.3
14:51:00	−16:15:00	2019/09/25/23:30	21.0	1.3
14:51:00	−18:15:00	2019/09/25/23:31	21.0	1.3
14:51:00	−20:15:00	2019/09/25/23:32	21.0	1.3
14:59:00	−16:15:00	2019/09/25/23:33	21.0	1.3
14:59:00	−18:15:00	2019/09/25/23:34	21.0	1.3
14:49:00	−17:30:00	2019/09/26/23:30	21.0	1.3
14:49:00	−19:30:00	2019/09/26/23:31	21.0	1.3
14:49:00	−15:30:00	2019/09/26/23:32	21.0	1.3
14:58:00	−15:30:00	2019/09/26/23:33	21.0	1.3
14:58:00	−17:30:00	2019/09/26/23:34	21.0	1.3
14:47:00	−17:30:00	2019/09/27/23:30	21.0	1.3
14:47:00	−19:30:00	2019/09/27/23:31	21.0	1.3
14:56:00	−17:30:00	2019/09/27/23:32	21.0	1.3
14:56:00	−19:30:00	2019/09/27/23:33	21.0	1.3
14:46:00	−17:30:00	2019/09/28/23:30	21.0	1.3
14:46:00	−19:30:00	2019/09/28/23:31	21.0	1.3
14:46:00	−21:15:00	2019/09/28/23:32	21.0	1.3
14:59:00	−21:15:00	2019/09/28/23:33	21.0	1.3
14:59:00	−19:30:00	2019/09/28/23:34	21.0	1.3
08:15:00	+14:00:00	2021/06/06/22:55	21.5	1.0
08:15:00	+16:00:00	2021/06/06/22:56	21.6	1.0
08:15:00	+12:00:00	2021/06/06/22:57	21.7	1.0
08:22:00	+16:00:00	2021/06/06/22:58	21.7	1.0
08:22:00	+14:00:00	2021/06/06/22:59	21.7	1.0
08:22:00	+12:00:00	2021/06/06/23:00	21.7	1.0
08:22:00	+17:00:00	2021/06/07/22:55	21.4	1.0
08:15:00	+10:00:00	2021/06/07/22:56	21.5	1.0
08:10:00	+08:00:00	2021/06/07/22:57	21.6	1.0
08:10:00	+10:00:00	2021/06/07/22:58	21.6	1.0
08:10:00	+12:00:00	2021/06/07/22:59	21.7	1.0
08:30:00	+16:00:00	2021/06/07/23:00	21.7	1.0
08:14:00	+16:00:00	2021/06/09/22:55	20.7	1.5
08:14:00	+14:00:00	2021/06/09/22:56	20.7	1.5
08:20:00	+17:50:00	2021/06/10/22:55	21.0	1.4
08:28:00	+18:10:00	2021/06/10/22:56	21.0	1.4
08:21:00	+10:34:00	2021/06/10/22:57	21.0	1.4
08:02:00	+10:00:00	2021/06/12/22:55	21.4	1.3
07:57:00	+08:00:00	2021/06/12/22:56	21.5	1.3
07:52:00	+06:04:00	2021/06/12/22:57	21.5	1.3
07:48:00	+04:00:00	2021/06/12/22:58	21.5	1.3
08:25:53	+10:32:00	2021/06/12/22:59	21.7	1.3
07:51:00	+02:00:00	2021/06/13/22:55	21.6	1.1
07:46:00	+00:01:00	2021/06/13/22:56	21.7	1.1
08:50:00	+12:34:00	2021/06/13/22:57	21.8	1.1
08:50:00	+14:30:00	2021/06/13/22:58	21.9	1.1
08:51:55	+19:50:00	2021/06/13/22:59	21.9	1.1
05:41:00	+06:00:00	2021/07/25/10:25	20.7	1.9
05:35:00	+08:00:00	2021/07/25/10:26	20.7	1.9
05:29:00	+10:00:00	2021/07/25/10:27	20.7	1.9
05:21:00	+12:00:00	2021/07/25/10:28	20.7	1.9
10:40:00	−01:00:00	2021/07/25/23:07	21.3	1.7
10:35:00	−03:00:00	2021/07/25/23:08	21.3	1.7
10:29:00	−05:00:00	2021/07/25/23:09	21.3	1.7
10:25:00	−07:00:00	2021/07/25/23:10	21.3	1.7
05:27:00	+13:00:00	2021/07/26/10:24	20.8	1.8

Table 1
(Continued)

R.A.(J2000) hh:mm:ss	Decl.(J2000) dd:mm:ss	UT Date YYYY/MM/DD/hh:mm	Limiting (mag)	Seeing (arcseconds)
05:19:30	+15:00:00	2021/07/26/10:25	20.8	1.8
05:11:00	+17:00:00	2021/07/26/10:26	20.8	1.8
05:04:00	+18:30:00	2021/07/26/10:27	20.8	1.8
11:07:30	+11:00:00	2021/07/26/23:05	21.1	1.6
11:07:30	+09:00:00	2021/07/26/23:06	21.4	1.6
11:02:00	+07:00:00	2021/07/26/23:07	21.4	1.6
10:57:00	+05:00:00	2021/07/26/23:08	21.4	1.6
10:51:00	+03:00:00	2021/07/26/23:09	21.4	1.6
10:47:00	+01:00:00	2021/07/26/23:10	21.4	1.6
05:57:00	+05:00:00	2021/07/27/10:25	20.3	1.9
06:01:30	+03:00:00	2021/07/27/10:26	20.3	1.9
06:09:30	+01:00:00	2021/07/27/10:27	20.3	1.9
11:17:00	+12:30:00	2021/07/27/23:06	20.1	2.5
10:39:30	−01:00:00	2021/07/27/23:07	20.5	2.5
10:36:30	−03:00:00	2021/07/27/23:08	20.5	2.5
11:06:30	+04:00:00	2021/07/27/23:09	20.5	2.5
11:12:30	+06:00:00	2021/07/27/23:10	20.5	2.5
06:29:00	−05:00:00	2021/07/28/10:25	21.1	1.6
06:25:00	−03:00:00	2021/07/28/10:26	21.1	1.6
06:19:30	−01:00:00	2021/07/28/10:27	21.1	1.6
07:11:00	−05:00:00	2021/08/10/10:13	20.9	1.3
07:21:00	−06:10:00	2021/08/11/10:20	21.0	1.4
07:15:00	−03:00:00	2021/08/11/10:21	21.0	1.4
07:10:00	−01:00:00	2021/08/11/10:22	21.0	1.4
07:35:00	−08:00:00	2021/08/13/10:18	20.6	1.4
07:40:00	−10:00:00	2021/08/13/10:19	20.4	1.4
11:45:00	−03:00:00	2021/08/13/23:08	20.5	1.7
11:51:50	−02:46:10	2021/08/14/23:09	20.4	1.6
11:57:30	−01:00:00	2021/08/14/23:10	20.4	1.6
12:02:30	+01:00:00	2021/08/14/23:11	20.4	1.6
12:37:00	−10:00:00	2021/08/28/23:21	21.8	1.4
12:41:00	−08:00:00	2021/08/28/23:22	21.8	1.4
12:46:00	−06:00:00	2021/08/28/23:23	21.8	1.4
12:54:20	−04:00:00	2021/08/28/23:24	21.8	1.4
12:59:30	−02:00:00	2021/08/28/23:25	21.8	1.4
13:05:10	−00:10:00	2021/08/28/23:26	21.8	1.4
12:43:00	−12:00:00	2021/08/29/23:22	21.1	1.9
12:38:38	−09:35:55	2021/08/29/23:23	21.1	1.9
13:08:53	−02:27:30	2021/08/29/23:24	21.1	1.9
13:17:00	+01:40:00	2021/08/30/23:25	20.2	2.2
13:22:00	+03:25:00	2021/08/30/23:26	20.2	2.2
12:50:00	−16:00:00	2021/08/31/23:23	19.9	1.6
12:45:00	−18:00:00	2021/08/31/23:24	19.9	1.6
14:12:00	−06:00:00	2021/09/16/23:29	20.7	1.5
14:12:30	−08:00:00	2021/09/16/23:30	21.0	1.5
14:08:00	−10:00:00	2021/09/16/23:31	21.0	1.5
14:04:00	−12:00:00	2021/09/16/23:32	21.0	1.5
14:12:00	−14:00:00	2021/09/19/23:31	20.0	2.6
14:17:00	−18:20:00	2021/09/22/23:31	21.2	1.3
14:20:00	−16:40:00	2021/09/22/23:32	21.2	1.3
14:24:00	−15:00:00	2021/09/22/23:33	21.2	1.3
14:28:00	−13:20:00	2021/09/22/23:34	21.2	1.3
15:06:00	−07:30:00	2021/09/27/23:31	21.6	1.3
15:02:00	−09:20:00	2021/09/27/23:32	21.6	1.3
14:57:00	−11:10:00	2021/09/27/23:33	21.6	1.3
15:45:00	−27:00:00	2021/10/16/23:50	21.0	1.4
16:02:00	−21:00:00	2021/10/16/23:52	21.3	1.4
15:58:00	−23:00:00	2021/10/16/23:53	21.3	1.4
15:54:00	−25:00:00	2021/10/16/23:54	21.3	1.4
16:26:00	−13:00:00	2021/10/19/23:50	21.0	1.2

Table 1
(Continued)

R.A.(J2000) hh:mm:ss	Decl.(J2000) dd:mm:ss	UT Date YYYY/MM/DD/hh:mm	Limiting (mag)	Seeing (arcseconds)
16:27:00	−15:00:00	2021/10/19/23:51	21.2	1.2
16:24:00	−17:00:00	2021/10/19/23:52	21.2	1.2
16:20:00	−19:00:00	2021/10/19/23:53	21.2	1.2
10:29:00	−05:00:00	2021/10/20/08:52	20.7	1.9
10:33:00	−07:00:00	2021/10/20/08:53	20.7	1.9
10:38:00	−09:00:00	2021/10/20/08:54	20.7	1.9
10:45:00	−11:00:00	2021/10/21/08:51	21.0	1.7
10:49:00	−13:00:00	2021/10/21/08:52	21.0	1.7
10:53:00	−15:00:00	2021/10/21/08:53	21.0	1.7
16:09:00	−34:00:00	2021/10/22/23:50	21.4	1.2
16:16:00	−32:00:00	2021/10/22/23:51	21.7	1.2
16:16:00	−30:00:00	2021/10/22/23:52	21.7	1.2
16:19:00	−28:20:00	2021/10/22/23:53	21.7	1.2
11:02:00	−17:00:00	2021/10/23/08:48	20.2	1.8
11:06:00	−19:00:00	2021/10/23/08:49	20.2	1.8
11:10:00	−21:00:00	2021/10/23/08:50	20.2	1.8
10:41:00	−04:00:00	2021/10/25/08:46	21.6	1.1
10:35:00	−02:00:00	2021/10/25/08:47	21.6	1.1
10:30:00	−00:10:00	2021/10/25/08:48	21.6	1.1
11:19:00	−07:00:00	2021/11/04/08:39	20.6	1.9
11:24:30	−09:00:00	2021/11/04/08:40	20.6	1.9
11:29:00	−11:00:00	2021/11/04/08:41	20.6	1.9
11:39:00	−13:00:00	2021/11/04/08:46	20.4	1.9
11:51:30	−15:00:00	2021/11/07/08:41	20.0	1.7
11:56:00	−17:00:00	2021/11/07/08:42	20.0	1.7
12:00:00	−19:00:00	2021/11/07/08:43	20.0	1.7
20:39:00	−26:00:00	2021/12/16/00:45	21.3	1.3
20:57:00	−20:00:00	2021/12/16/00:46	21.5	1.3
20:53:30	−22:00:00	2021/12/16/00:47	21.5	1.3
20:50:00	−24:00:00	2021/12/16/00:48	21.5	1.3
14:14:00	−20:00:00	2021/12/16/08:20	21.7	1.1
14:18:30	−22:00:00	2021/12/16/08:21	21.7	1.1
14:23:00	−24:00:00	2021/12/16/08:22	21.7	1.1
14:32:00	−26:00:00	2021/12/16/08:27	21.4	1.1
20:45:20	−32:00:00	2021/12/19/00:46	20.8	1.8
20:52:00	−30:30:00	2021/12/19/00:48	21.0	1.8
20:53:30	−29:00:00	2021/12/19/00:49	21.0	1.8
20:56:30	−27:30:00	2021/12/19/00:50	21.0	1.8
14:42:00	−27:30:00	2021/12/19/08:22	21.0	1.8
14:44:30	−29:00:00	2021/12/19/08:23	21.0	1.8
14:46:00	−30:30:00	2021/12/19/08:24	21.0	1.8
14:52:00	−32:00:00	2021/12/19/08:27	20.8	1.8
21:24:20	−15:30:00	2021/12/22/00:47	21.1	1.5
21:27:00	−17:00:00	2021/12/22/00:48	21.3	1.5
21:25:00	−18:30:00	2021/12/22/00:49	21.3	1.5
21:22:30	−20:00:00	2021/12/22/00:50	21.3	1.5
21:20:00	−21:30:00	2021/12/22/00:51	21.3	1.5
14:32:00	−16:00:00	2021/12/22/08:25	21.0	1.8
14:36:00	−17:30:00	2021/12/22/08:26	21.0	1.8
14:40:00	−19:00:00	2021/12/22/08:27	21.0	1.8
14:47:00	−20:30:00	2021/12/22/08:28	20.8	1.8
14:49:00	−22:00:00	2021/12/23/08:25	21.4	1.3
14:52:00	−23:30:00	2021/12/23/08:26	21.4	1.3
14:55:00	−25:00:00	2021/12/23/08:27	21.4	1.3
15:00:00	−26:30:00	2021/12/23/08:28	21.2	1.3
21:08:00	−29:00:00	2021/12/24/00:47	21.3	1.2
21:17:00	−27:30:00	2021/12/24/00:48	21.6	1.2
21:20:00	−26:00:00	2021/12/24/00:49	21.6	1.2
21:23:00	−24:30:00	2021/12/24/00:50	21.6	1.2
21:26:00	−23:00:00	2021/12/24/00:51	21.6	1.2

Table 1
(Continued)

R.A.(J2000) hh:mm:ss	Decl.(J2000) dd:mm:ss	UT Date YYYY/MM/DD/hh:mm	Limiting (mag)	Seeing (arcseconds)
15:04:00	−28:00:00	2021/12/24/08:25	21.4	1.1
15:07:00	−29:30:00	2021/12/24/08:26	21.4	1.1
15:08:00	−31:15:00	2021/12/24/08:27	21.4	1.1
15:13:00	−33:00:00	2021/12/24/08:31	21.1	1.1
15:26:00	−34:00:00	2021/12/28/08:28	21.6	1.2
15:26:30	−35:30:00	2021/12/28/08:29	21.6	1.2
15:27:00	−37:00:00	2021/12/28/08:30	21.6	1.2
15:32:00	−38:30:00	2021/12/28/08:34	21.3	1.2
15:40:00	−40:00:00	2021/12/31/08:30	21.8	1.1
15:40:30	−41:40:00	2021/12/31/08:31	21.8	1.1
15:41:30	−43:30:00	2021/12/31/08:32	21.8	1.1
15:47:00	−45:00:00	2021/12/31/08:35	21.5	1.1
22:07:00	−20:00:00	2022/01/03/00:52	21.1	1.2
15:37:00	−20:00:00	2022/01/03/08:34	22.0	1.1
15:41:00	−21:30:00	2022/01/03/08:35	22.0	1.1
15:45:00	−23:00:00	2022/01/03/08:36	21.9	1.1
15:51:00	−24:30:00	2022/01/03/08:41	21.6	1.1
16:02:00	−26:00:00	2022/01/06/08:34	22.0	0.9
16:05:30	−27:30:00	2022/01/06/08:35	22.0	0.9
16:08:30	−29:00:00	2022/01/06/08:36	21.9	0.9
16:14:00	−30:30:00	2022/01/06/08:40	21.7	1.0
16:15:00	−32:00:00	2022/01/06/08:41	21.6	1.0
16:15:30	−25:00:00	2022/01/09/08:37	21.2	1.9
16:13:30	−23:30:00	2022/01/09/08:38	20.8	2.2
16:11:00	−22:00:00	2022/01/09/08:39	20.9	2.1
16:12:00	−20:30:00	2022/01/09/08:44	20.4	2.0
16:10:00	−19:00:00	2022/01/09/08:45	20.5	1.8
22:43:00	−24:30:00	2022/01/13/00:58	21.3	1.2
16:33:30	−24:00:00	2022/01/13/08:47	21.5	0.9
16:31:30	−22:30:00	2022/01/13/08:48	21.6	0.9
16:30:00	−21:00:00	2022/01/13/08:49	21.5	0.9
16:29:00	−19:00:00	2022/01/13/08:53	21.3	0.9
16:28:00	−17:30:00	2022/01/13/08:54	21.2	0.9
16:43:16	−17:32:15	2022/01/18/08:49	21.1	1.4
23:20:00	−20:00:00	2022/01/21/00:49	21.3	1.3
23:23:30	−18:30:00	2022/01/21/00:50	21.4	1.3
23:27:00	−17:00:00	2022/01/21/00:51	21.5	1.3
23:30:30	−15:30:00	2022/01/21/00:52	21.5	1.3
16:55:15	−17:34:30	2022/01/21/08:50	21.5	1.2
17:03:00	−19:00:00	2022/01/21/08:51	21.5	1.2
17:06:00	−20:30:00	2022/01/21/08:52	21.4	1.2
17:12:00	−21:30:00	2022/01/21/08:57	21.2	1.2
17:15:00	−23:00:00	2022/01/21/08:58	21.1	1.2
17:02:00	−16:00:00	2022/01/22/08:52	21.2	1.5
16:59:30	−14:30:00	2022/01/22/08:53	21.2	1.5
16:57:30	−13:00:00	2022/01/22/08:54	21.2	1.5
17:03:40	−17:34:30	2022/01/23/08:55	21.8	1.1
16:57:00	−11:00:00	2022/01/23/08:57	21.8	1.1
17:14:30	−17:00:00	2022/01/24/08:54	21.4	1.3
16:59:50	−09:40:00	2022/01/24/08:55	21.4	1.3
16:59:00	−08:00:00	2022/01/24/08:58	21.2	1.3

3. Results

Using DECam, we covered 624 square degrees of sky near to and interior to Venus' orbit. Three new NEOs were discovered, with two likely being about 1 km or larger in size (Table 2). In addition, we serendipitously detected several known NEOs moving well over 90 arcseconds per hour, including Atira-, Aten-, Amor-, and Apollo-type NEOs, with several being Potentially Hazardous Asteroids (PHAs).

3.1. 2021 PH27: Atira Type

Asteroid 2021 PH27 was discovered by S. Sheppard on 2021 August 13 in twilight images taken near the Sun by the Local

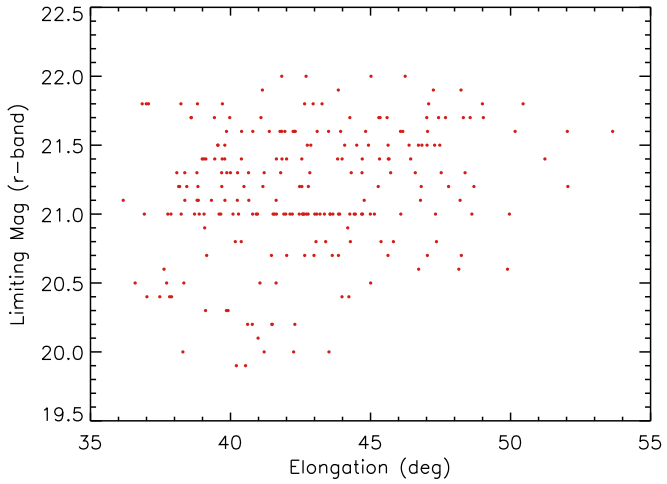

Figure 5. The limiting magnitude of each twilight field vs. its elongation distance from the Sun. Most of the fields had a limiting magnitude above 21 mag in the *r* band, with the best fields reaching nearly 22nd mag.

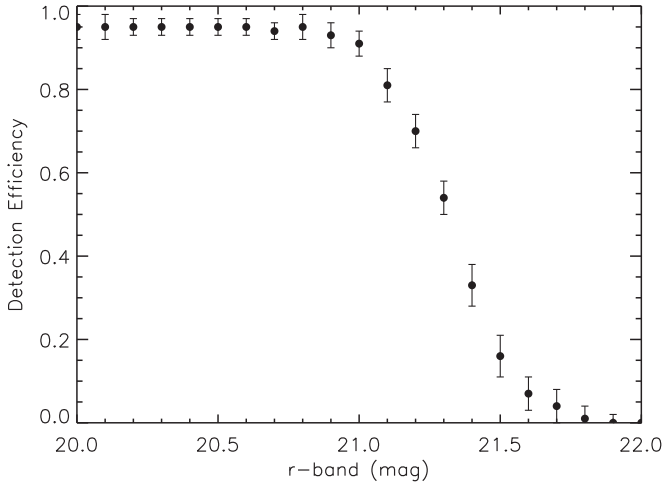

Figure 6. The moving object detection efficiency for the survey for a typical field with 1.″4 seeing. The typical field limiting magnitude was around 21.3 mag in the *r* band. Table 1 and Figure 5 shows the limiting magnitude of each field of the DECam twilight survey.

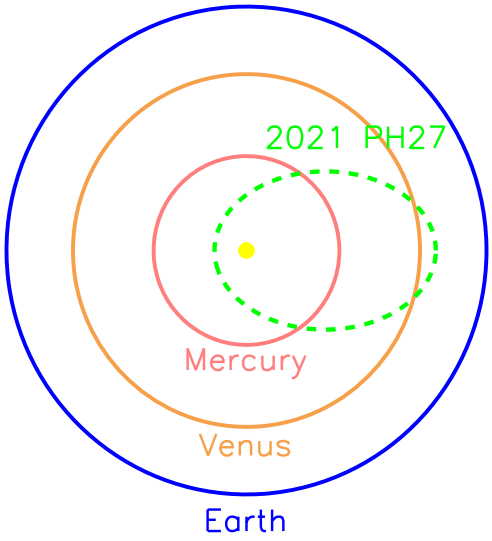

Figure 7. The orbit of the newly discovered Atira asteroid 2021 PH27, which has the smallest semimajor axis of any known asteroid. Though it orbits the Sun faster than Venus as its semimajor axis is less than that of Venus, 2021 PH27 has an aphelion exterior to Venus. It also has a perihelion interior to Mercury's orbit, causing 2021 PH27 to experience the largest general relativistic effects from the Sun's gravity of any object known in the solar system.

Table 2
New Asteroid Discoveries

Name	*a* (au)	*e*	*i* (deg)	*H* (mag)	Diam (km)	Type
2021 LJ4	0.676	0.382	9.827	20.1	0.3 − 0.6	Atira
2021 PH27	0.4617	0.712	31.927	17.7	0.9 − 1.7	Atira
2022 AP7	2.924	0.715	13.835	17.1	1.1 − 2.3	Apollo

Note. Orbital elements are from the Minor Planet Center as of 2022 June, with the end number being the significant digit of the uncertainty. Though the albedos are unknown, they are likely between 5% and 20% as many NEOs are in this range (Pravec et al. 2012). Using the standard 14% albedo assumption for unknown albedo NEOs, as used by the NASA Center for Near Earth Object Studies, this means an absolute magnitude brighter than 17.75 mag is likely larger than 1 km in size. The diameter range shown above is assuming 20% and 5% albedos, respectively.

Volume Complete Cluster Survey (LoVoCCS; Dell'Antonio 2020; Fu et al. 2022) in collaboration with the DECam twilight asteroid survey (Sheppard et al. 2021). The asteroid was recovered the next night on August 14 at both the Baade–Magellan telescope and again using DECam on the Blanco 4 m telescope. As the object was relatively bright at 19.2 mag, it could be tracked by 1 meter class telescopes. On August 15 the asteroid was observed by DECam and Magellan as well as the Las Cumbres 1 m telescopes in South Africa and Chile. It was tracked with 1 m class telescopes for almost a month. In addition, pre-discovery images of the asteroid were found from DECam archival images on 2017 July 16, allowing the orbit to be well determined. 2021 PH27 was also recovered again in March 2022.

2021 PH27 has the smallest semimajor axis of any known asteroid and thus the shortest orbital period for an asteroid of about 113 days (Table 2). Only the planet Mercury has a smaller known semimajor axis for any object in our solar system. 2021 PH27 has an Atira-type asteroid orbit that always keeps it inside of Earth's orbit (Figure 7). Because 2021 PH27 has a fairly eccentric orbit, it crosses both the orbits of Mercury and Venus and approaches the Sun to within about 0.133 au.

To understand the orbital behavior of 2021 PH27, we ran a numerical orbital simulation using the SWIFT RMVS4 integrator described by Levison & Duncan (1994) and included the planets Mercury, Venus, Earth+Moon (barycenter), Mars (barycenter), Jupiter (barycenter), Saturn (barycenter), Uranus (barycenter), and Neptune (barycenter). The time step of the simulations was 0.1 days. We generated 1000 clones using the JPL covariance matrix of 2021 PH27 from 2022 April 18. The randomly generated points follow a six-dimensional normal distribution defined by the covariance matrix and the orbital elements as described by Namouni & Morais (2018).

The orbit of 2021 PH27 is dynamically unstable within a few million year timescale (Figures 8 and 9). There is a 0.7% chance that it will collide with Venus in the next million years, and it will pass within Venus' Hill sphere in the next 950 to 1050 yr, as all of our clones travel through Venus' Hill sphere

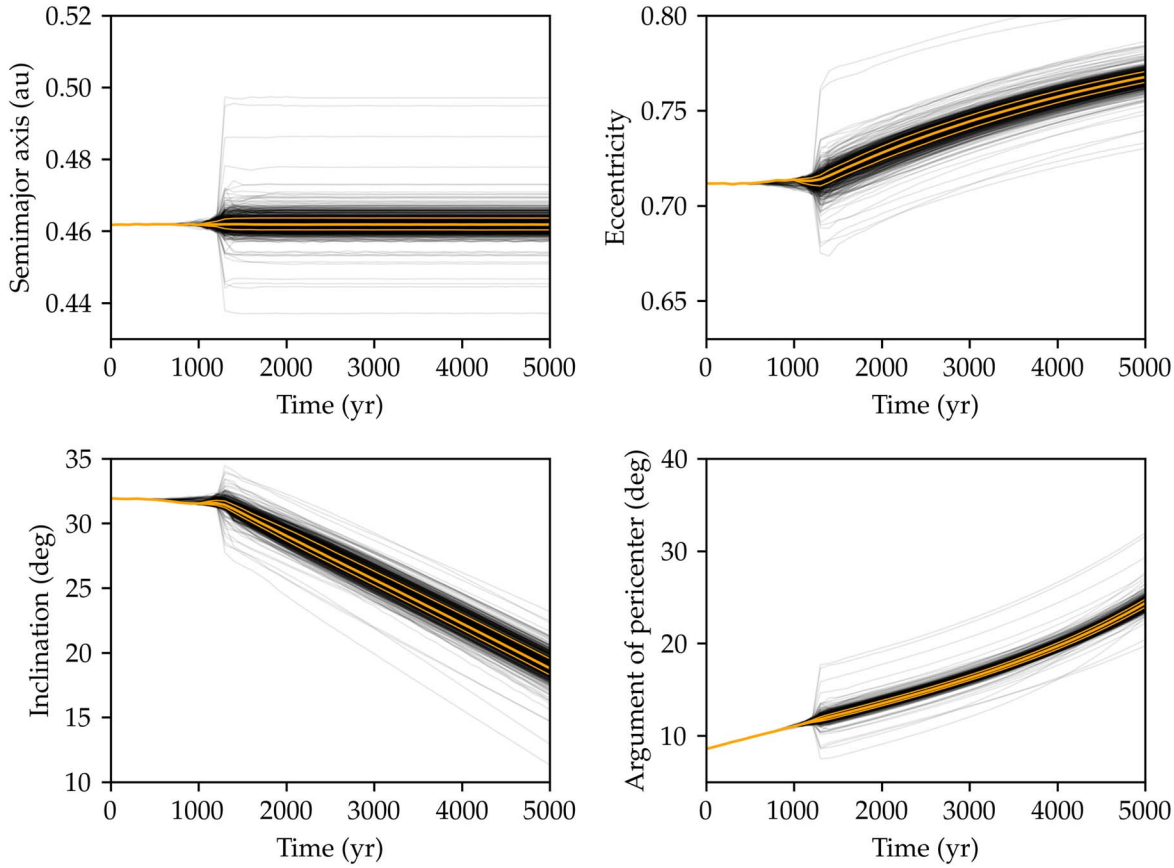

Figure 8. The orbital stability of 2021 PH27 over a few thousand years. Each gray line shows one of the 1000 clone particles of 2021 PH27's orbital parameters. The bold middle yellow line shows the median orbital parameters of 2021 PH27 and the thin yellow lines the 1σ of the median value. The orbit is dynamically unstable and 2021 PH27 has numerous close encounters with Venus. The first close encounter with Venus occurs around the year 3000 AD (or 950–1050 yr from now or time zero). This close encounter with Venus creates a noticable spread in the asteroid clones of 2021 PH27, as most of these clones get inside of Venus' Hill sphere during the encounter, modifying the orbit of 2021 PH27 depending on how close it gets to the planet.

in that time. 2021 PH27's very close perihelion to the Sun means 2021 PH27 experiences the largest general relativistic effects on any known object in our solar system, including Mercury. We used the ReboundX code to determine the general relativistic effects on 2021 PH27 from the Sun (Tamayo et al. 2020). The orbital precession rate of 2021 PH27 is about 53 arcseconds per century, which is faster than Mercury's orbital precession rate of about 43 arcseconds per century (Will 2018). The general relativity effects are not important in 2021 PH27's orbital evolution as planetary perturbations are much more significant. The asteroid interacts strongly with Venus and is likely in some sort of Kozai–Lidov oscillation from Jupiter and/or the inner planets as seen by the coupling of the eccentricity and inclination of the evolution of 2021 PH27's orbit in Figure 9 (Kozai 1962; Lidov 1962; de la Fuente Marcos & de la Fuente Marcos 2021). 2021 PH27's orbit and Venus overlap enough that it is a PHA to Venus with a Venus Minimum Orbit Intersection Distance (MOID) of only 0.015. If 2021 PH27 is or becomes an active asteroid, it could create meteor showers in Venus' atmosphere (Albino et al. 2022).

2021 PH27 can reach surface temperatures of around 500°C during its closest approach to the Sun. This means its surface has been strongly thermally processed over time and its internal structure likely has been heavily stressed from the intense and changing thermal environment (Li & Jewitt 2013; Lisse & Steckloff 2022).

2021 PH27 was relatively bright at discovery, being some 19.2 mag in the *r* band. As the aphelion distance is only 0.79 au, which is just beyond Venus' orbit, this object, though relatively bright and around 1 km in size, would be very hard for most NEO surveys to find as they generally do not observe near Venus' orbit or interior to it. The large inclination of about 32° also means 2021 PH27 spends most of its time well away from the ecliptic.

Though 2021 PH27 most likely came from the main asteroid belt, it is possible that it could have originated much closer to the Sun from a possible stable reservoir of small objects in resonance with Venus or even the hypothetical Vulcanoid population, which is a theoretical stable area of small bodies interior to Mercury (Greenstreet et al. 2012).

3.2. 2021 LJ4: Atira Type

2021 LJ4 was found in twilight images taken on 2021 June 6 using DECam (Sheppard & Tholen 2021). The object was recovered again using DECam on 2021 June 8 as well as on 2021 June 9 and 11 using the CFHT telescope on Maunakea. Additional recoveries were later made using DECam. The object was faint at 21.4 mag in the *r* band at discovery. The asteroid appears to be a typical Atira type with a period of 0.55 yr and an aphelion just interior to Earth's orbit at 0.93 au, with it crossing the orbits of both Venus and Mercury (Table 2). 2021 LJ4 was recovered in 2021 November as well as 2022

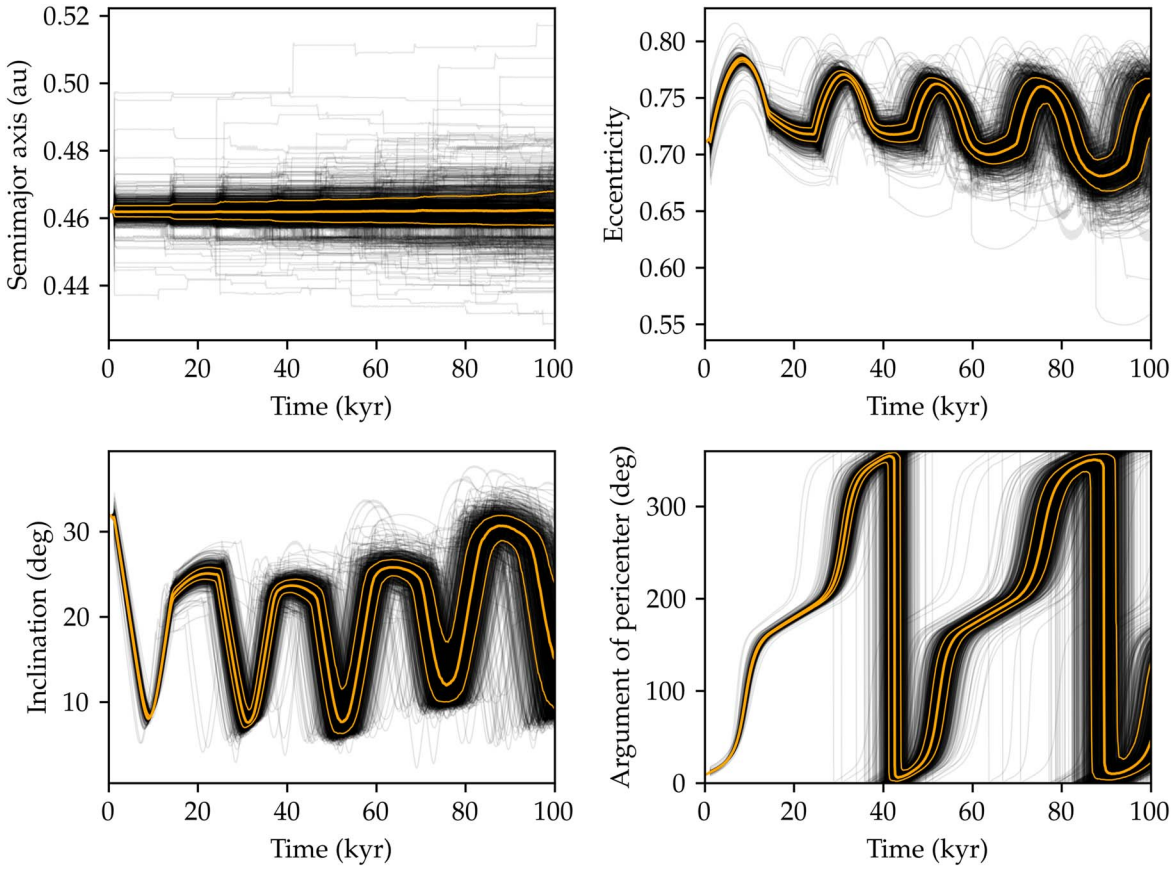

Figure 9. Same as Figure 8 but now showing the numerical orbital simulation of 2021 PH27 out to 100,000 yr. The orbit of 2021 PH27 is dynamically unstable over a few million years with numerous close encounters with Venus. The coupling of the eccentricity and inclination over time suggests 2021 PH27 is experiencing a resonant interaction with the planets.

May, yielding a well-determined orbit for the object. Assuming a moderate S-type asteroid albedo, the object is likely to be 300 to 400 m in diameter. Though 2021 LJ4 has only a moderate inclination, its Atira orbit and somewhat small size make it hard for most NEO surveys using smaller telescopes to detect this asteroid, making it an ideal discovery using DECam during twilight observing.

3.3. 2022 AP7: Apollo Type

The object 2022 AP7 was discovered using DECam in twilight on 2022 January 13 (Sheppard 2022). It was recovered using DECam a few nights later on 2022 January 16 using the asteroid short-arc orbit and ephemeris computation program (known as KNOBS) written by Tholen & Whiteley (2000). Recovery occurred again using DECam on the nights of 2022 January 18, 21, and 23. After recovery a few weeks later using the Las Cumbres telescopes and the University of Hawaii 88 inch telescope, 2022 AP7 was found in data from 2017 in both the NEO Pan-STARRS and Catalina Sky Survey images, when the object was last near opposition, though far from Earth and thus faint. The orbit is thus very well known based on a ∼5 year observation arc. 2022 AP7 is an Apollo-type NEO which crosses Earth's orbit with a perihelion near 0.83 au and aphelion near Jupiter at 5.0 au (Table 2).

The Earth MOID for 2022 AP7 is only 0.0475 au, making it a PHA and likely the largest PHA found since 2014 based on absolute magnitude. 2022 AP7 is likely to be in the top 5% of the largest PHAs known. 2022 AP7 was relatively faint at discovery being 20.8 mag, but because it was relatively far from Earth at about 1.9 au and distant from the Sun around 1.4 au. It is a fairly large object, likely being well over 1 km in size assuming a moderate albedo (1.0–2.3 km diameter for an albedo of 0.25–0.05, respectively).

Such a large object with an orbital period of only 5 yr and only a moderate inclination might be expected to have been found earlier by one of the NEO surveys that cover most of the sky exterior to Earth's orbit. Thus either 2022 AP7 has an orbit that aliases Earth's orbit, keeping it usually at a large distance from Earth when in the night sky near opposition, or 2022 AP7 may be brightening as it comes to perihelion from cometary effects. 2022 AP7 was found as it approached perihelion, which is when cometary activity is expected to increase significantly. In our discovery and recovery images, no obvious coma or tail was detected. As the orbital period of 2022 AP7 is near exactly 5 yr, it does have an orbit that currently aliases with Earth's, keeping it well away from Earth when near opposition for now, meaning it would only be efficiently found in a twilight type survey as it would be near the Sun and brightest only when Earth is more on the other side of the Sun and its elongation very low. Thus 2022 AP7 is a discovery that exemplifies how a relatively large telescope observing toward the Sun during twilight can find large NEOs that most of the current NEO surveys do not efficiently find. Many of the "missing" yet-to-be-found ∼1 km sized NEOs likely have orbits that alias with Earth, making them distant and faint when in the night sky at opposition like 2022 AP7.

4. Discussion

The main design of the survey was to find or put constraints on the population and orbital properties of objects near to or interior to Venus' orbit. We did not find any relatively stable Venus co-orbital or resonant objects, allowing us to put strong upper limits on the size of such a population if it exists. Though not the main goal of the survey, four Atira-type asteroids were detected, which is ∼15% of the known Atira population. This allows us to put significant constraints on the size of the Atira population, which have orbits completely interior to Earth's. In addition, this survey is one of the few that can put modest constraints on the Vatira population, which has orbits completely interior to Venus' orbit.

To determine what percentage of each interior population's orbits we may have surveyed, we performed several Monte Carlo simulations. These simulations consisted of generating 100,000 clones of orbits of a particular population and then determining how many of these objects our survey would have been expected to detect based on the fields observed, limiting magnitude of each field, and the efficiency of the survey. This gives a rough percentage of the entire population of orbits. We then use Poisson statistics to put limits or upper limits, in the case of no detections, of each population simulated.

For each simulation we assumed asteroids of six spectral types (S-type with 0.22 albedo, M with 0.17, E with 0.45, C with 0.06, P with 0.04, and D with 0.05; Mainzer et al. 2011, 2012; Shevchenko et al. 2016; Morbidelli et al. 2020) and three diameters ($D = 0.5$, 1.0, and 1.5 km) using the same methods as detailed by Pokorny et al. (2020). See Pokorny et al. (2020) for more details on our simulations, including the phase function, apparent visual magnitude, and diameter conversions we used in our simulations. The asteroid type and hence the albedo of the asteroid only matters for detecting objects less than 1 km as all objects, no matter their type, would have similar detection efficiencies near or above 1 km as our survey was deep enough to make almost all 1 km or bigger inner asteroids efficiently detected.

4.1. Stable Venus Resonant Objects

Pokorny & Kuchner (2019) found that some low-eccentricity, low-inclination Venus co-orbital objects could be in resonance and stable for the age of the solar system. If this population exists, it would be a very interesting population to find and study as these objects could be the remnant of the inner solar system's formation disk. Pokorny et al. (2020) performed a limited survey with DECam of the space near Venus' orbit to put modest constraints on this possible population of stable Venus resonant co-orbitals. Here we extend the Pokorny et al. (2020) analysis using the new, much larger survey area covered near Venus' orbit with DECam. For this population we followed 100,000 clones of low-eccentricity, low-inclination Venus co-orbital asteroids that were shown to be stable for the age of the solar system by Pokorny & Kuchner (2019).

Based on our simulations, this DECam twilight survey should have observed some 21%–23% of the entire population of stable Venus co-orbitals larger than 1 km, which depends on the spectral type and thus albedo of the objects (Table 3). Since we found no relatively stable Venus resonant objects and there are none known, this population is not likely to be very large. We calculate the upper limit on the population size of 1 km or larger stable Venus co-orbitals to be only about 4^{+6}_{-3}, depending on the asteroid type (Table 3). Similar constraints are found for even smaller 0.5 km sized higher albedo asteroids types like the S, M, and E types, as they would be relatively easier to find because of their high reflectance. For the darker asteroid types, like the C, P, and D types, smaller sized asteroids of 0.5 km are basically unconstrained as most would be too faint for our survey to detect efficiently (Table 3).

Table 3
Stable Venus Co-orbital Completeness Percentage and Population

Type	$D = 0.5$ (km)	$D = 1.0$ (km)	$D = 1.5$ (km)
S-type	$22\%(4^{+6}_{-3})$	$23\%(4^{+6}_{-3})$	$23\%(4^{+6}_{-3})$
M-Type	$21\%(4^{+7}_{-3})$	$23\%(4^{+6}_{-3})$	$23\%(4^{+6}_{-3})$
E-Type	$23\%(4^{+6}_{-3})$	$23\%(4^{+6}_{-3})$	$23\%(4^{+6}_{-3})$
C-Type	$0.8\%(100^{+170}_{-80})$	$21\%(4^{+7}_{-3})$	$23\%(4^{+6}_{-3})$
P-Type	$0.2\%(540^{+900}_{-400})$	$20\%(4^{+8}_{-3})$	$23\%(4^{+6}_{-3})$
D-Type	$0.4\%(210^{+350}_{-150})$	$21\%(4^{+7}_{-3})$	$23\%(4^{+6}_{-3})$

Note. Survey completeness based on a Monte Carlo simulation of our survey for each population in percent assuming the shown diameter (D) or larger and asteroid type. In "()" is the computed upper limit on the population size based on our survey coverage and null result.

Table 4
Unstable Venus Co-orbital Completeness Percentage and Population

Type	$D = 0.5$ (km)	$D = 1.0$ (km)	$D = 1.5$ (km)
S-type	$8\%(10^{+16}_{-7})$	$10\%(8^{+13}_{-6})$	$10\%(8^{+13}_{-6})$
M-Type	$6\%(12^{+20}_{-9})$	$10\%(8^{+13}_{-6})$	$10\%(8^{+13}_{-6})$
E-Type	$10\%(8^{+13}_{-6})$	$10\%(8^{+13}_{-6})$	$10\%(8^{+13}_{-6})$
C-Type	$0.4\%(220^{+360}_{-170})$	$7\%(11^{+17}_{-7})$	$10\%(8^{+13}_{-6})$
P-Type	$0.2\%(440^{+720}_{-330})$	$5\%(14^{+23}_{-10})$	$9\%(8^{+13}_{-6})$
D-Type	$0.3\%(310^{+510}_{-230})$	$7\%(11^{+19}_{-8})$	$10\%(8^{+13}_{-6})$

Note. Survey completeness based on a Monte Carlo simulation of our survey for each population in percent assuming the shown diameter or larger and asteroid type. In "()" is the computed upper limit on the population size based on our survey coverage and null result.

4.2. Unstable Venus Near Co-orbitals

There are five well observed asteroids that currently have orbital periods similar to Venus: (322756) 2001 CK32, (524522) 2002 VE68, 2012 XE133, 2013 ND15, and 2015 WZ12. All of these, as well as the newer objects found since 2020 are much smaller than 1 km and are on dynamically unstable orbits on the order of a few million years, as discussed in Section 1. We generated 100,000 clones using the above five object's semimajor axes, eccentricities, and inclinations by randomly selecting the remaining orbital elements. Though we did not observe any of these known objects, through this simulation, we find our survey would have detected about 5%–10% of the objects similar to these known dynamically unstable Venus near co-orbitals and larger than 1 km in size, depending on their albedos and spectral types (Table 4). From this simulation there could be a few of these near unstable Venus co-orbitals to discover around the 1 km size regime.

Table 5
Atira/Apohele Asteroid Population Completeness Percentage and Population

Type	$D = 0.5$ (km)	$D = 1.0$ (km)	$D = 1.5$ (km)
S-type	7%(55 ± 30)	8%(50 ± 25)	8%(50 ± 25)
M-Type	6%(65 ± 35)	8%(50 ± 25)	8%(50 ± 25)
E-Type	8%(50 ± 25)	8%(50 ± 25)	8%(50 ± 25)
C-Type	0.4%(950 ± 500)	7%(60 ± 30)	8%(50 ± 25)
P-Type	0.3%(1500 ± 800)	6%(75 ± 35)	8%(50 ± 25)
D-Type	0.3%(1200 ± 600)	6%(65 ± 30)	8%(50 ± 25)

Note. Survey completeness based on a Monte Carlo simulation of our survey for each population in percent assuming the shown diameter (D) or larger and asteroid type. In "()" is the computed upper limit on the population size based on our survey coverage and finding four Atira asteroids within the survey.

4.3. Atira/Apohele Asteroid Population

In addition to the two new Atira asteroids discovered in this survey, 2021 LJ4 and 2021 PH27, we also detected serendipitously the previously known Atira asteroids 2019 AQ3 and 2021 BS1. We used the semimajor axis, eccentricity, and inclination of the 25 known Atira objects with well-determined orbits as of 2022 March and randomly selected the other orbital elements to generate 100,000 clones. Table 5 shows the percentage of the population of Atira objects our survey should have detected, which amounts to 5%–8% of the total population larger than 1 km, depending on the albedos of the objects.

Our simulations show there are about 50 to 75 ± 35 Atiras that are about 1 km or larger (Table 5), suggesting less than half of the largest objects in the Atira population have been found to date. Assuming there are about 1000 NEOs of 1 km or larger, this would make the Atira population about 5% of the NEO population. This result generally agrees with estimates of the Atira population size from some earlier NEO models (Bottke et al. 2002; Greenstreet et al. 2012), but is somewhat higher than the currently modeled ∼1% for the Atira population fraction of NEOs (Granvik et al. 2018).

These results are based on low number statistics and mostly assumed albedos, so if the population size of 1 km Atira objects is on the low end of the uncertainty, than there are likely only a few large Atiras left to find. The larger undiscovered Atira asteroids that remain probably have high inclinations and/or smaller than average semimajor axes and/or eccentricities, which would keep them mostly well interior to Earth's orbit and away from the darker skies where the main NEO surveys operate most efficiently. This is true for the 1 km sized Atira 2021 PH27, which we found with a high inclination and very low semimajor axis (Table 2).

4.4. Vatira Asteroid Population

Vatira asteroids have orbits completely interior to Venus' orbit. Since the Vatira population's orbital distribution is still highly uncertain, we simulated two different Vatira populations to understand how sensitive our survey would be to finding Vatira asteroids. First, we used the semimajor axis, eccentricity, and inclination of the only known Vatira asteroid (594913) 'Ayló'chaxnim (2020 AV2) and generated 100,000 clones by randomly selecting the remaining orbital elements. In this simulation, we would have found about 5% of the ∼1 km or larger Vatira asteroids with similar orbits as 2020 AV2 (Table 6). This puts only minimal constraints on a Vatira population with orbits like 2020 AV2, as there could still be tens of objects like 2020 AV2 to be found since they spend most of their time at smaller elongations than many of our survey fields.

Table 6
Vatira Asteroids like 2020 AV2 Population Completeness Percentage

Type	$D = 0.5$ (km)	$D = 1.0$ (km)	$D = 1.5$ (km)
S-type	$5\%(17^{+30}_{-13})$	$5\%(16^{+30}_{-12})$	$5\%(16^{+30}_{-12})$
M-Type	$5\%(19^{+30}_{-15})$	$5\%(16^{+30}_{-12})$	$5\%(16^{+30}_{-12})$
E-Type	$5\%(16^{+30}_{-12})$	$5\%(16^{+30}_{-12})$	$5\%(16^{+30}_{-12})$
C-Type	$0.7\%(130^{+220}_{-100})$	$5\%(18^{+30}_{-14})$	$5\%(16^{+30}_{-12})$
P-Type	$0.5\%(170^{+270}_{-130})$	$5\%(19^{+30}_{-15})$	$5\%(16^{+30}_{-12})$
D-Type	$0.5\%(160^{+270}_{-120})$	$5\%(19^{+30}_{-15})$	$5\%(16^{+30}_{-12})$

Note. Survey completeness based on a Monte Carlo simulation of our survey for each population in percent assuming the shown diameter (D) or larger and asteroid type. In "()" is the computed upper limit on the population size based on our survey coverage and null result.

Table 7
Circular Vatira Asteroid Population Completeness Percentage

Type	$D = 0.5$ (km)	$D = 1.0$ (km)	$D = 1.5$ (km)
S-type	1%	1%	1%
M-Type	1%	1%	1%
E-Type	1%	1%	1%
C-Type	0.3%	0.9%	1%
P-Type	0.3%	0.9%	1%
D-Type	0.3%	0.9%	1%

Note. Survey completeness based on a Monte Carlo simulation of our survey for each population in percent assuming the shown diameter (D) or larger and asteroid type.

In a second simulation, we made a 100,000 asteroid hypothetical Vatira population by creating a somewhat circular and moderately inclined population through randomly selecting orbital elements with $0.50 < a < 0.60$ au, $0.0 < e < 0.1$, and $0 < i < 15°$ and randomly selecting the other remaining orbital elements between 0 and 360°. As many of the objects in this hypothetical Vatira population would not have elongations as great as 2020 AV2, it would be much harder to detect these objects in our fields. Thus our survey would only find at most about 1% of objects in this hypothetical Vatira population (Table 7).

5. Conclusions and Summary

The twilight survey using DECam on the CTIO Blanco 4 m telescope is one of the largest area and sensitive searches ever performed for objects interior to Earth's and near Venus' orbit. Though no objects with orbits similar to or interior to Venus' orbit were found, the survey did find three relatively large NEOs, including two Atira and one Apollo orbital type. The new discovery 2021 PH27 is about 1 km in size and has the smallest semimajor axis and thus shortest orbital period around the Sun of any known asteroid. 2021 PH27 has strong interactions with Venus, with it likely passing through Venus' Hill sphere in 950–1050 yr from now, making it a PHA to Venus. The eccentric orbit of 2021 PH27 means it crosses both Mercury's and Venus' orbit and its very low perihelion of only

0.13 au creates about a 53 arcsecond per century precession in its orbit from general relativistic effects, which are the largest known in our solar system. The newly discovered 2022 AP7 is an Apollo-type NEO that is probably the largest potentially hazardous NEO to Earth found in several years, being some 1.5 km in size. There are likely several more 1 km sized Atira-type asteroids left to find, which probably have low semimajor axes and high inclinations, like 2021 PH27, making them hard to find for most asteroid surveys. The DECam twilight survey is covering sky geometries and areas that most other surveys do not cover to depths not usually obtained, filling an important niche in the survey for the last few remaining relatively large unknown NEOs. Interestingly, the twilight survey has discovered more larger asteroids ($\gtrsim$1 km) than smaller ones even though the survey is sensitive to smaller asteroids. This might suggest the smaller asteroids are dynamically less stable and/or more susceptible to break-up from the extreme thermal and gravitational environment near the Sun, though additonal discoveries of asteriods with orbits near the Sun must be made to determine statistically if the smaller asteroids are under-abundant since in general they are also harder to detect.

Observations were obtained at Cerro-Tololo Inter-American Observatory, National Optical Astronomy Observatory, which are operated by the Association of Universities for Research in Astronomy, under contract with the National Science Foundation. This project used data obtained with the Dark Energy Camera (DECam), which was constructed by the Dark Energy Survey (DES) collaborating institutions: Argonne National Lab, University of California Santa Cruz, University of Cambridge, Centro de Investigaciones Energeticas, Medioambientales y Tecnologicas-Madrid, University of Chicago, University College London, DES-Brazil consortium, University of Edinburgh, ETH-Zurich, University of Illinois at Urbana-Champaign, Institut de Ciencies de l'Espai, Institut de Fisica d'Altes Energies, Lawrence Berkeley National Lab, Ludwig-Maximilians Universitat, University of Michigan, National Optical Astronomy Observatory, University of Nottingham, Ohio State University, University of Pennsylvania, University of Portsmouth, SLAC National Lab, Stanford University, University of Sussex, and Texas A&M University. Funding for DES, including DECam, has been provided by the U.S. Department of Energy, National Science Foundation, Ministry of Education and Science (Spain), Science and Technology Facilities Council (UK), Higher Education Funding Council (England), National Center for Supercomputing Applications, Kavli Institute for Cosmological Physics, Financiadora de Estudos e Projetos, Fundação Carlos Chagas Filho de Amparo a Pesquisa, Conselho Nacional de Desenvolvimento Científico e Tecnológico and the Ministério da Ciência e Tecnologia (Brazil), the German Research Foundation-sponsored cluster of excellence "Origin and Structure of the Universe" and the DES collaborating institutions. D.T. was supported by NASA grant 80NSSC21K0807. P.P. was supported by NASA ISFM EIMM award, the NASA Cooperative Agreement 80GSFC21M0002 and NASA solar system Workings award 80NSSC21K0153. T.S.R. acknowledges funding from the NEO-MAPP project (H2020-EU-2-1-6/870377). C.M. was partially supported by the international Gemini Observatory, a program of NSF's NOIRLab, which is managed by the Association of Universities for Research in Astronomy (AURA) under a cooperative agreement with the National Science Foundation, on behalf of the Gemini partnership of Argentina, Brazil, Canada, Chile, the Republic of Korea, and the United States of America. This work was (partially) funded by the Spanish MICIN/AEI/10.13039/501100011033 and by "ERDF A way of making Europe" by the "European Union" through grant RTI2018-095076-B-C21, and the Institute of Cosmos Sciences University of Barcelona (ICCUB, Unidad de Excelencia María de Maeztu') through grant CEX2019-000918-M. This work makes use of observations from the Las Cumbres Observatory global telescope network. This paper includes data gathered with the 6.5 m Magellan Telescopes located at Las Campanas Observatory, Chile.

ORCID iDs

Scott S. Sheppard https://orcid.org/0000-0003-3145-8682
David J. Tholen https://orcid.org/0000-0003-0773-1888
Petr Pokorný https://orcid.org/0000-0002-5667-9337
Marco Micheli https://orcid.org/0000-0001-7895-8209
Ian Dell'Antonio https://orcid.org/0000-0003-0751-7312
Shenming Fu https://orcid.org/0000-0001-5422-1958
Chadwick A. Trujillo https://orcid.org/0000-0001-9859-0894
Rachael Beaton https://orcid.org/0000-0002-1691-8217
Scott Carlsten https://orcid.org/0000-0002-5382-2898
Alex Drlica-Wagner https://orcid.org/0000-0001-8251-933X
Clara Martínez-Vázquez https://orcid.org/0000-0002-9144-7726
Sidney Mau https://orcid.org/0000-0003-3519-4004
Toni Santana-Ros https://orcid.org/0000-0002-0143-9440
Luidhy Santana-Silva https://orcid.org/0000-0003-3402-6164
Cristóbal Sifón https://orcid.org/0000-0002-8149-1352
Sunil Simha https://orcid.org/0000-0003-3801-1496
Audrey Thirouin https://orcid.org/0000-0002-1506-4248
David Trilling https://orcid.org/0000-0003-4580-3790
A. Katherina Vivas https://orcid.org/0000-0003-4341-6172
Alfredo Zenteno https://orcid.org/0000-0001-6455-9135

References

Albino, C., Tanga, P., & Bernardi, F. 2022, MNRAS, 511, 40
Bolin, B., Masci, F., Ye, Q., et al. 2020, MPEC 2020-A99
Bolin, B. T., Ahumada, T., van Dokkum, P., et al. 2022, MNRAS, Advance Access
Bottke, W., Morbidelli, A., Jedicke, R., et al. 2002, Icar, 156, 399
Brasser, R., Innanen, K., Connors, M., et al. 2004, Icar, 171, 102
Connors, M., Wiegert, P., & Veillet, C. 2011, Natur, 475, 481
de la Fuente Marcos, C., & de la Fuente Marcos, R. 2012, MNRAS, 427, 728
de la Fuente Marcos, C., & de la Fuente Marcos, R. 2013, MNRAS, 432, 886
de la Fuente Marcos, C., & de la Fuente Marcos, R. 2014, MNRAS, 439, 2970
de la Fuente Marcos, C., & de la Fuente Marcos, R. 2017, RNAAS, 1, 3
de la Fuente Marcos, C., & de la Fuente Marcos, R. 2020, MNRAS, 494, 6
de la Fuente Marcos, C., & de la Fuente Marcos, R. 2021, RNAAS, 5, 205
Dell'Antonio, I. 2020, NOIRLab Mirror, 1, 14
Flaugher, B., Diehl, H., Honscheid, K., et al. 2015, AJ, 150, 150
Fu, S., Dell'Antonio, I., Chary, R., et al. 2022, ApJ, 933, 84
Granvik, M., Morbidelli, A., Jedicke, R., et al. 2016, Natur, 530, 303
Granvik, M., Morbidelli, A., Jedicke, R., et al. 2018, Icar, 312, 181
Granvik, M., Morbidelli, A., Vokrouhlicky, D., et al. 2017, A&A, 598, 52
Greenstreet, S. 2020, MNRAS, 493, L129
Greenstreet, S., Ngo, H., & Gladman, B. 2012, Icar, 217, 355
Harris, A., & Chodas, P. 2021, Icar, 365, 114452
Hui, M., Wiegert, P., Tholen, D., & Fohring, D. 2021, ApJ, 922, 25
Jedicke, R., Bolin, B., Granvik, M., & Beshore, E. 2016, Icar, 266, 173
Jones, M., Bewsher, D., & Brown, D. 2013, Sci, 342, 960
Kozai, Y. 1962, AJ, 67, 591

Leinert, C., & Moster, B. 2007, A&A, 472, 335
Levison, H., & Duncan, M. 1994, Icar, 108, 18
Li, J., & Jewitt, D. 2013, AJ, 145, 154
Lidov, M. 1962, P&SS, 9, 719
Lisse, C., & Steckloff, J. 2022, Icar, 381, 114995
Mainzer, A., Bauer, J., Grav, T., et al. 2014, ApJ, 784, 110
Mainzer, A., Grav, T., Bauer, J., et al. 2011, ApJ, 743, 156
Mainzer, A., Grav, T., Masiero, J., et al. 2012, ApJ, 752, 110
Malhotra, R. 2019, NatAs, 3, 193
Masiero, J., Mainzer, A., Bauer, J., et al. 2020, PSJ, 1, 5
Mikkola, S., Brasser, R., Wiegert, P., & Innanen, K. 2004, MNRAS, 351, 63
Morais, M., & Morbidelli, A. 2006, Icar, 185, 29
Morbidelli, A., Delbo, M., Granvik, M., et al. 2020, Icar, 340, 113631
Myhrvold, N. 2016, PASP, 128, 5004
Namouni, F., & Morais, M. 2018, MNRAS, 477, 117
Pokorny, P., & Kuchner, M. 2019, ApJL, 873, L16
Pokorny, P., & Kuchner, M. 2021, PSJ, 2, 193
Pokorny, P., Kuchner, M., & Sheppard, S. 2020, PSJ, 1, 47
Pravec, P., Harris, A. W., Kušnirák, P., Galád, A., & Hornoch, K. 2012, Icar, 221, 365
Santana-Ros, T., Micheli, M., Faggioli, L., et al. 2022, Nature Comm., 13, 447
Schunova-Lilly, E., Jedicke, R., Veres, P., Denneau, L., & Wainscoat, R. 2017, Icar, 284, 114
Sergeyev, A., & Carry, B. 2021, A&A, 652, 59
Sheppard, S. 2012, AJ, 144, 169
Sheppard, S. 2022, MPEC 2022-B21
Sheppard, S., & Tholen, D. 2021, MPEC 2021-L125
Sheppard, S., & Trujillo, C. 2009, Icar, 202, 12
Sheppard, S., Trujillo, C., Tholen, D., & Kaib, N. 2019, AJ, 157, 139
Sheppard, S., Dell'Antonio, I., Fu, S., et al. 2021, MPEC 2021-Q41
Shevchenko, V., Belskaya, I., Muinonen, K., et al. 2016, P&SS, 123, 101
Smith, J., Tucker, D., Kent, S., et al. 2002, AJ, 123, 2121
Strom, R., Malhotra, R., Xiao, Z., et al. 2015, RAA, 15, 407
Tamayo, D., Hanno, R., Pengshuai, S., & Hernandez, D. 2020, MNRAS, 491, 2885
Tholen, D., & Whiteley, R. 2000, BAAS, 32, 1018
Trujillo, C., Jewitt, D., & Luu, J. 2001, AJ, 122, 457
Will, C. 2018, Phys. Rev. Lett., 120, 191101
Ye, Q., & Granvik, M. 2019, ApJ, 873, 104
Ye, Q., Masci, F., Ip, W., et al. 2020, AJ, 159, 70